Electrochimica Acta 133 (2014) 146–152

Contents lists available at ScienceDirect

Electrochimica Acta

journal homepage: www.elsevier.com/locate/electacta

$LiNi_{0.5}Mn_{1.5}O_4$ Thin-Film Cathodes on Gold-Coated Stainless Steel Substrates: Formation of Interlayers and Electrochemical Properties

Michael Gellert[a,*], Katharina I. Gries[b], Julia Zakel[a], Andrea Ott[b], Stefan Spannenberger[a], Chihiro Yada[c], Fabio Rosciano[c], Kerstin Volz[b], Bernhard Roling[a]

[a] Department of Chemistry, Structure & Technology Research Laboratory, University of Marburg, Hans-Meerwein-Strasse, D–35032 Marburg, Germany
[b] Structure & Technology Research Laboratory, University of Marburg, Hans-Meerwein-Strasse, D–35032 Marburg, Germany
[c] Advanced Technology 1 Division, Toyota Motor Europe, Hoge Wei 33, B - 1930 Zaventem, Belgium

ARTICLE INFO

Article history:
Received 17 February 2014
Received in revised form 27 March 2014
Accepted 28 March 2014
Available online 6 April 2014

Keywords:
High voltage spinel cathodes
Thin-films
Electrochemical impedance spectroscopy
ToF-SIMS
STEM/EDX

ABSTRACT

Thin films of $LiNi_{0.5}Mn_{1.5}O_4$ (LNMO) were prepared on gold-coated stainless steel substrates via a poly(vinylpyrrolidone)-based sol-gel process. Films with a thickness in the range of 1 μm were found to exhibit a capacity close to the theoretical one. The formation of interlayers (i) between the LNMO films and the LP30 electrolyte (mixture of dimethyl carbonate (DMC) and ethylene carbonate (EC) (1:1 v/v) containing 1 $mol \cdot l^{-1} LiPF_6$) and (ii) between the LNMO films and the gold-coated substrate was studied by means of electrochemical impedance spectroscopy (EIS), time-of-flight secondary-ion mass-spectrometry (ToF-SIMS), and scanning transmission electron microscopy together with energy dispersive X-ray spectroscopy (STEM/EDX). The combination of these methods turns out to be very powerful for understanding the chemical composition and properties of interlayers and for identifying the origin of semicircles in Nyquist impedance plots. At the LNMO/LP30 interface, we observe an interlayer (solid electrolyte interface, SEI) with a thickness of about 50 nm, while at the LNMO/gold interface, a mixed oxide layer with a thickness in the range of 250 nm is found. The mixed oxide layer is caused by diffusion of Cr and Ni from the stainless steel through the gold layer. While the LNMO/LP30 interlayer contributes significantly to the interfacial impedance, the impedance of the LNMO/gold interlayer seems to be negligible, despite its larger thickness.

1. Introduction

Nowadays, lithium-ion batteries are an integral part of our mobile life. They power not only laptops and mobile phones, but also electrical vehicles (EV) are equipped with this type of battery. For EV applications, battery cells with increased gravimetric and, in particular, volumetric energy density have to be developed. Here, all-solid-state batteries are promising [1,2], since compact multilayer battery structures can be prepared. In addition, the usage of non-flammable solid electrolytes improves safety issues.

The cathode materials used in such batteries should exhibit a high capacity and a high redox potential vs. Li^+/Li. A promising material is $LiNi_{0.5}Mn_{1.5}O_4$ (LNMO), which crystallizes in a spinel structure allowing for three-dimensional Li^+ ion transport.[3] LNMO exhibits a redox potential of 4.7 V vs Li^+/Li and a capacity around 130 $mAhg^{-1}$ in composite cathodes and up to 148 $mAhg^{-1}$ as a thin-film material without additives.[4–6] While the mass production of composite battery electrodes with carbon additives and polymeric binders is well established, thin-film electrodes are mostly prepared via costly sputtering techniques. A cheaper alternative is sol-gel chemistry combined with spin or dip coating.[7] Here, liquid organic precursors are coated onto a substrate and are converted to oxides via a heating process. High temperatures of about 700 °C are needed to form crystalline oxides. However, many metallic substrates used as current collectors cannot withstand such high temperatures in air. In basic research, pure gold current collectors were used successfully.[8–10] As a cheaper alternative, we have deposited Au layers onto stainless steel substrates.

The electrochemical performance of cathode material can suffer from SEI formation at the cathode/electrolyte interface as well as from dissolution of metal ions in the liquid electrolyte. In various studies, these effects were investigated for composite LNMO electrodes containing graphite. The formation of metal fluorides on the LNMO surface and of polyethylene carbonate on the graphite surface [11–13] were observed. Caroll *et al.* [14] studied thin-film LNMO cathodes by means of X-ray photoelectron spectroscopy and

* Corresponding author.
E-mail address: michael.gellert@chemie.uni-marburg.de (M. Gellert).

http://dx.doi.org/10.1016/j.electacta.2014.03.184
0013-4686/

did not detect any SEI formation. In contrast, Mohamedi *et al.* [5] carried out electrochemical impedance spectroscopy (EIS) measurements on thin-film LNMO samples in a three-electrode setup and found an impedance contribution, which they attributed to the impedance of the "solid-liquid interface". However from the EIS results alone, this interpretation is ambiguous. Alternatively, it is thinkable that an interlayer at the LNMO/current collector interface is responsible for the observed process. Recently, Norberg *et al.* [15] produced a binder-free electrode by simply pressing LNMO powder onto an aluminum foil. They investigated dissolution effects by means of fluorescence spectroscopy and found electrolyte decomposition and partial dissolution of the SEI.

All these studies do not yet provide a unique picture about interlayers at the LNMO/electrolyte and at the LNMO/current collector interface, respectively, and about the impact of such interlayers on the electrochemical performance. In this paper, we show that the combination of EIS with time-of-flight secondary-ion mass-spectrometry (ToF-SIMS) and scanning transmission electron microscopy/energy dispersive X-ray spectroscopy (STEM/EDX) provides valuable additional information about the formation and chemical composition of interlayers as well as about the impedance of the interlayers. Thin LNMO films prepared on gold-coated stainless steel substrates were first characterized in-situ in contact to a LP30 electrolyte by means of charge/discharge measurements and EIS. After completing the electrochemical measurements, the cells were disassembled, and the cathode multilayer structure was investigated by means of ToF-SIMS and STEM/EDX. Our results provide clear evidence that interlayers are formed at both interfaces, however with different contributions to the cell impedance.

2. Experimental

The Poly(vinylpyrrolidone) route (PVP route) was used for the preparation of a uniform solution. The starting materials were the following: PVP powder with an average molecular weight of 25,000 g/mol, $Li(CH_3COO)$ x 2 H_2O, $Ni(CH_3COO)_2 \times 4$ H_2O, $Mn(CH_3COO)_2 \times 4$ H_2O, CH_3COOH, *i*-C_3H_7OH, H_2O (molar ratio = 0.94: 0.69: 0.34: 0.94: 25.05: 28.19: 43.85). All starting materials, except the PVP powder (Roth), were obtained from Aldrich. The materials were mixed, heated to 50 °C and stirred for 6 hours to obtain a clear turquoise solution.

The metal substrate was prepared by electrochemical deposition of gold onto chromium-nickel steel (X5CrNi18-10, V2A). Before deposition, the steel surface was mechanically polished (0.25 μm diamond paste, MD-CHEM polishing pad). The electrolytes used for the gold deposition were "WILAPLAT Haftgoldbad AC3 SSF" (Wieland) for the adhesive layer and "WILAPLAT Goldplattierbad 750 SC" (Wieland) for obtaining a smooth surface. The overall thickness of the Au layer was about 2 μm.

Spin coating of the gel onto the substrates was carried out with a rotation speed of 3000 rpm. The gel film was converted to a ceramic oxide by heating to 600 °C in air for 4 minutes. The spin coating and heating steps were repeated 10 and 20 times, respectively. In the following, the samples are denoted by LNMO10L (10-layer film) and LNMO20L (20-layer film). Finally, the films were heated to 700 °C for 8 minutes in air in order to form crystalline LNMO. The films thicknesses were determined by means of cross-sectional STEM. The LNMO20L and LNMO10L films exhibited a thickness around 1 μm and 500 nm, respectively. Samples for powder X-ray diffraction (XRD) (Philipps X'PERT, Cu-Kα) were obtained by heating 1 ml of the sol to 700 °C for 1 h in air.

ToF-SIMS measurements on the LNMO films were carried out using a time-of-flight secondary ion mass spectrometer (IONTOF GmbH). As primary ion source, a Bi^+ ion gun was used in high-current bunched mode (pulsed target current: 0.5 pA). For sputtering, a dual source column sputter gun (DSC-S) with O_2^+ as sputter species was used to produce a sputter crater with a size of 300 μm· 300 μm (sputter current around 200 nA). For analysis, the Bi^+ ions rastered over a 100 μm · 100 μm area in the center of the crater. A low energy electron gun (20 eV) was used for charge compensation. After the ToF-SIMS analysis, the crater depth was determined with a surface profilometer (Sloan Dektak 3ST, Veeco Instruments).

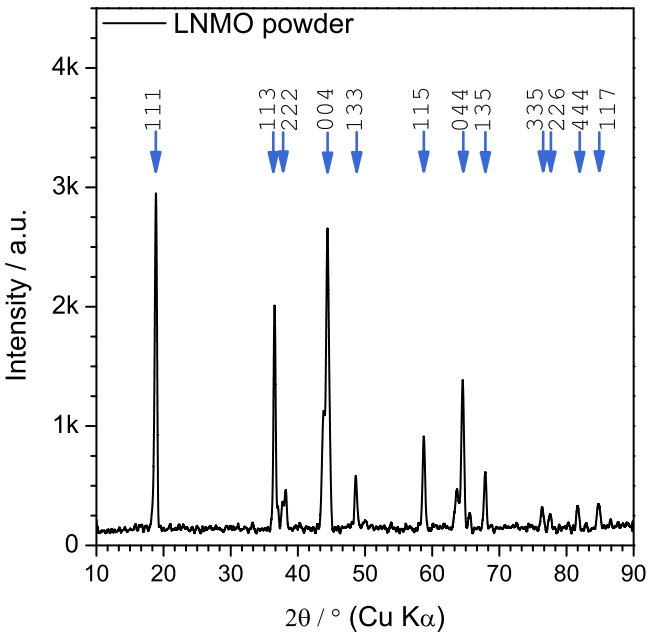

Fig. 1. Powder X-ray diffraction patterns of the $LiNi_{0.5}Mn_{1.5}O_4$ powders obtained via a sol-gel synthesis.

Surface morphology was analyzed by atomic force microscopy (AFM) (NT-MDT Solver P47) used in semi-contact mode.

STEM investigations have been performed on a double Cs corrected (scanning) transmission electron microscope (JEM 2200FS, JEOL) operating at 200 kV and equipped with an EDX detector (XFlash 5000, Bruker). To create cross-section samples thin enough for electron transparency, the lift-out method was used in a dual beam system (JIB 4601F, JEOL) which contains of a focused (gallium) ion beam (FIB) and a scanning electron microscope (SEM). As a protection layer for the FIB lamella a tungsten deposition was used.

Electrochemical measurements on the thin films were carried out at 25 °C in a two-electrode setup with lithium metal as counter electrode. To this end, a BioLogic SP-150 Potentiostat was used. LP30 (Merck) was chosen as electrolyte, and the electrodes were separated by 5 pieces of "Whatman GF/A" filters. Impedance measurements were performed at different dc voltages in a frequency range from 500 kHz to 100 mHz using an ac voltage of 10 mV_{rms}. In order to ensure an equilibrium state of the cell during each EIS measurement, the cell was potentiostatically polarized for 4 h before starting the EIS measurement. The obtained impedance data were analyzed using the home-made software suite "Relax Impedance Spectrum Analysis".

3. Results and Discussion

3.1. XRD and AFM

The XRD examination of the powders obtained from the sol proved the correct crystal structure (Fig. 1.). No significant impurities could be detected.

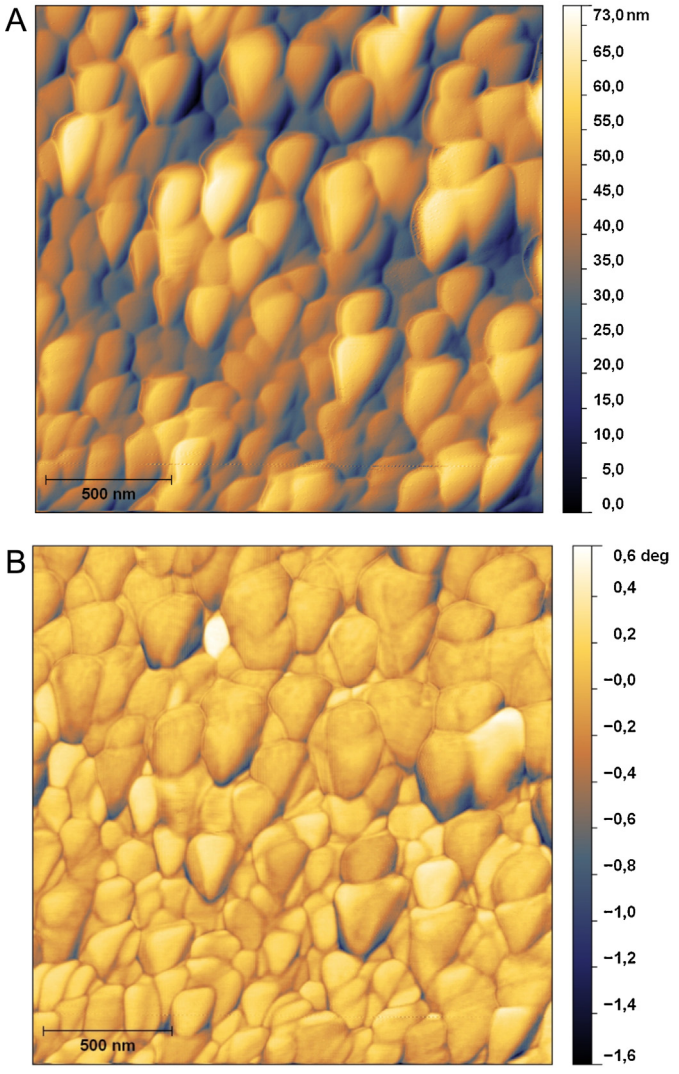

Fig. 2. a) AFM topographic image of the surface of freshly prepared $LiNi_{0.5}Mn_{1.5}O_4$ electrode (LNMO10L).b) AFM phase-contrast image of the freshly prepared $LiNi_{0.5}Mn_{1.5}O_4$ electrode surface (LNMO10L).

Standard AFM surface analysis of the thin films revealed a smooth surface with a broad distribution of grain sizes from about 50 nm up to about 300 nm. Representative topographic and phase contrast images of a LNMO10L sample are shown in Fig. 2a and b.

3.2. Charge/Discharge Measurements of Battery Cells

Battery cells with LNMO thin-film cathodes and lithium metal as counter electrode were charged and discharged twice using a current density of 100 μAcm^{-2}, before any other electrochemical measurements were done. This corresponds to a rate of 1 C–2 C, depending on sample thickness. The charge/discharge capacity was calculated using the electrode area of 1.13 cm^2 and the film thickness obtained from cross-section STEM images. During the first charging process, both samples exhibit a capacity which is larger than the theoretical capacity, see Fig. 3a and 3b. This overcharging is due to irreversible processes, most likely the formation of interlayers at the LNMO/electrolyte and the LNMO/current collector interface. Overcharging is particularly pronounced for the thinner film LNMO10L.

In the second cycle, the discharge capacity of thicker films LNMO20L is close to the theoretical value of 65.5 $\mu Acm^{-2}\,\mu m^{-1}$, which is based on the redox pairs $Ni^{2+/3+}$ and $Ni^{3+/4+}$ around

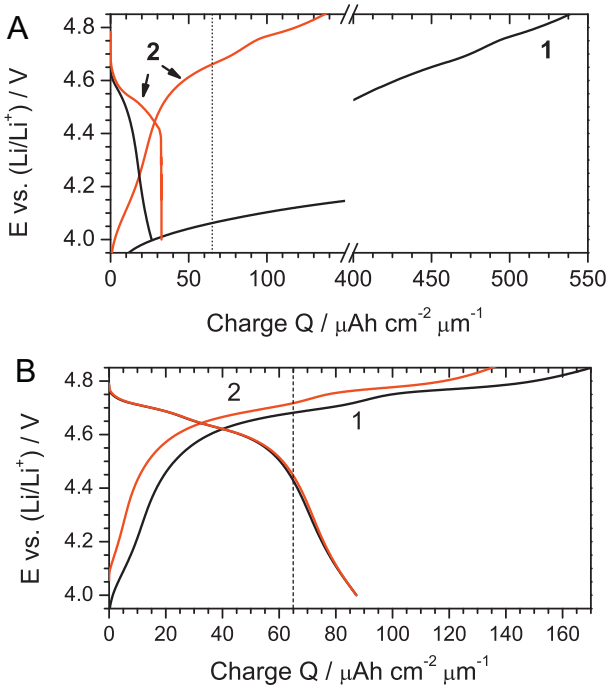

Fig. 3. Galvanostatic charge and discharge curves of LNMO films: a) LNMO10L film; b) LNMO20L film. Black lines: first cycle; red lines: second cycle.

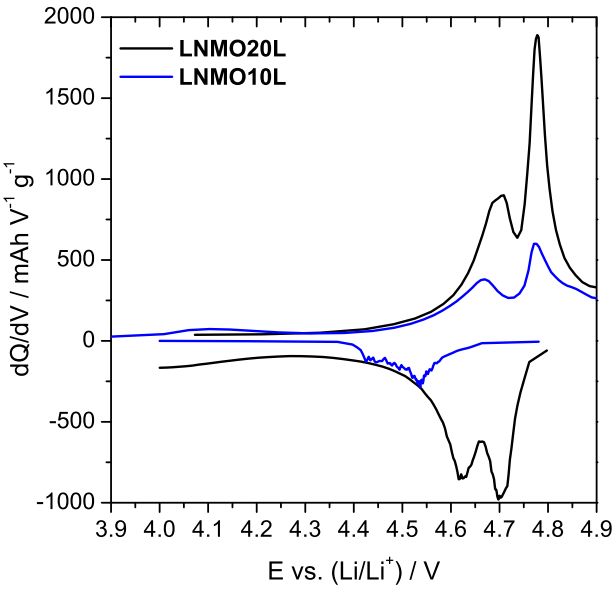

Fig. 4. dQ/dV-curves of both LNMO films derived from the second charge/discharge cycle.

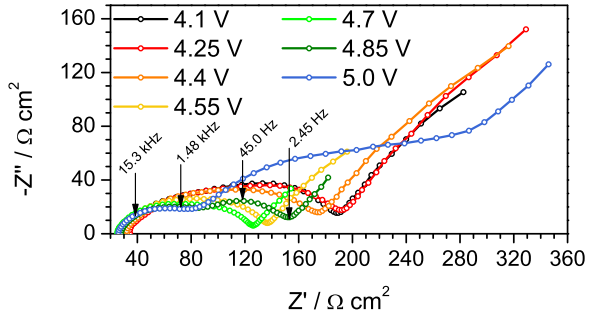

Fig. 5. Impedance spectra of a Li/LP30/LNMO20L cell at different cell voltages.

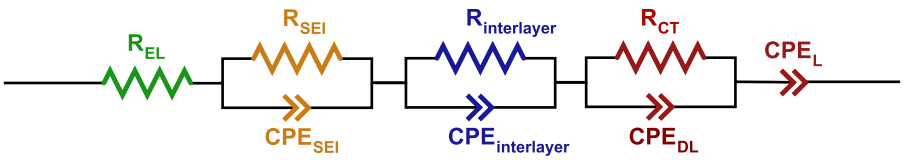

Fig. 6. Equivalent circuit for fitting the impedance spectra shown in Fig. 5.

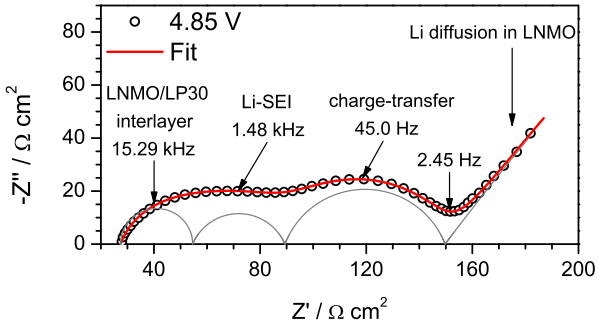

Fig. 7. Fitted impedance spectrum of a Li/LP30/LNMO20L cell at 4.85 V.

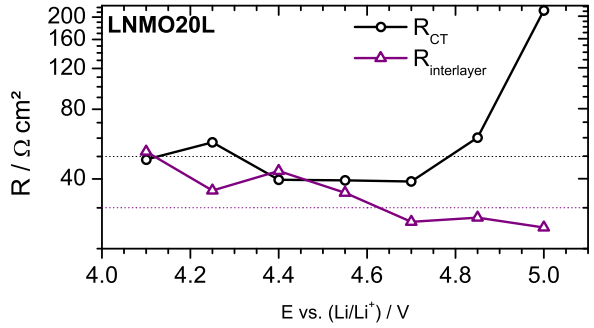

Fig. 8. Charge-transfer resistance and interlayer resistance of a Li/LP30/LNMO20L cell at different cell voltages.

4.7 V.The thinner LNMO10L films reach only 33 $\mu Acm^{-2}\,\mu m^{-1}$, which may be due to the loss of active material during overcharging in the first cycle.

In Fig. 4, derivative curves dQ/dV are shown, in which two redox peaks for $Ni^{2+/3+}$ and $Ni^{3+/4+}$, respectively, can be clearly distinguished. In addition, the derivative curves reveal a capacity contribution around 4 V, which is due to the presence of Mn^{3+} impurities (redox pair $Mn^{3+/4+}$). If the correct stoichiometry

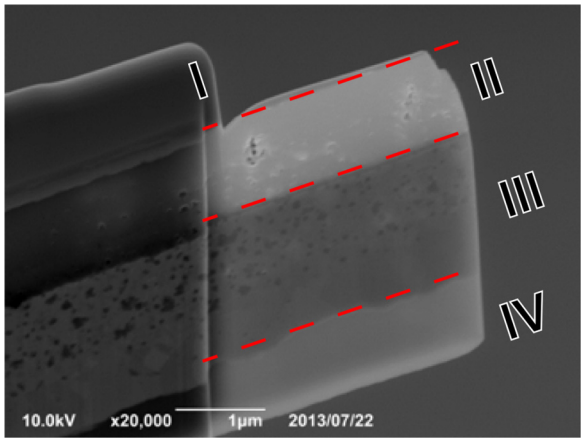

Fig. 10. SEM image of a LNMO20L lamella. For the preparation of the lamella, LNMO (II) was covered with a very thin tungsten layer (I) to prevent degradation and electrostatic charge during the ion milling. A gold layer (III) deposited on stainless steel (IV) was used as substrate.

$LiNi_{0.5}Mn_{1.5}O_4$ is obtained, all manganese ions exhibit an oxidation state +IV, and only $Ni^{2+/3+/4+}$redox activity is found. Mn reduction can be caused by a loss of nickel ions during the synthesis via the formation of $Ni(CO)_4$.[16]

3.3. Electrochemical Impedance Spectroscopy

Nyquist impedance plots of a cell with a LNMO20L thin-film cathode are shown at different cell voltages in Fig. 5. Four impedance contributions can be clearly distinguished: (i) a semicircle due to the SEI on the Li counter electrode. The impedance of this semicircle was determined by an independent EIS measurement on a symmetric Li | electrolyte | Li cell; (ii) a second semicircle partially overlapping with the Li-SEI semicircle, which is due to interlayers in the cathodic half cell; (iii) a cell voltage-dependent semicircle due to charge transfer in the cathodic half cell; (iv) a low-frequency spike, which is most likely caused by Li diffusion in the LNMO films.

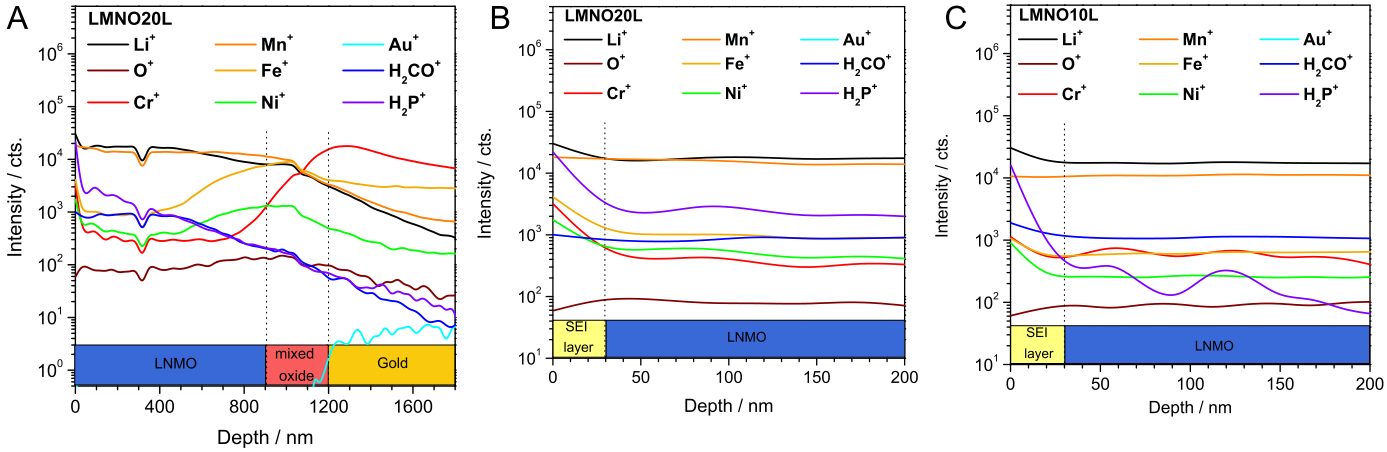

Fig. 9. a) ToF-SIMS depth profiles of a LNMO20L film. b) ToF-SIMS depth profiles of a LNMO20L film in the first 200 nm from the surface. c) ToF-SIMS depth profile of a LNMO10L film in the first 200 nm from the surface.

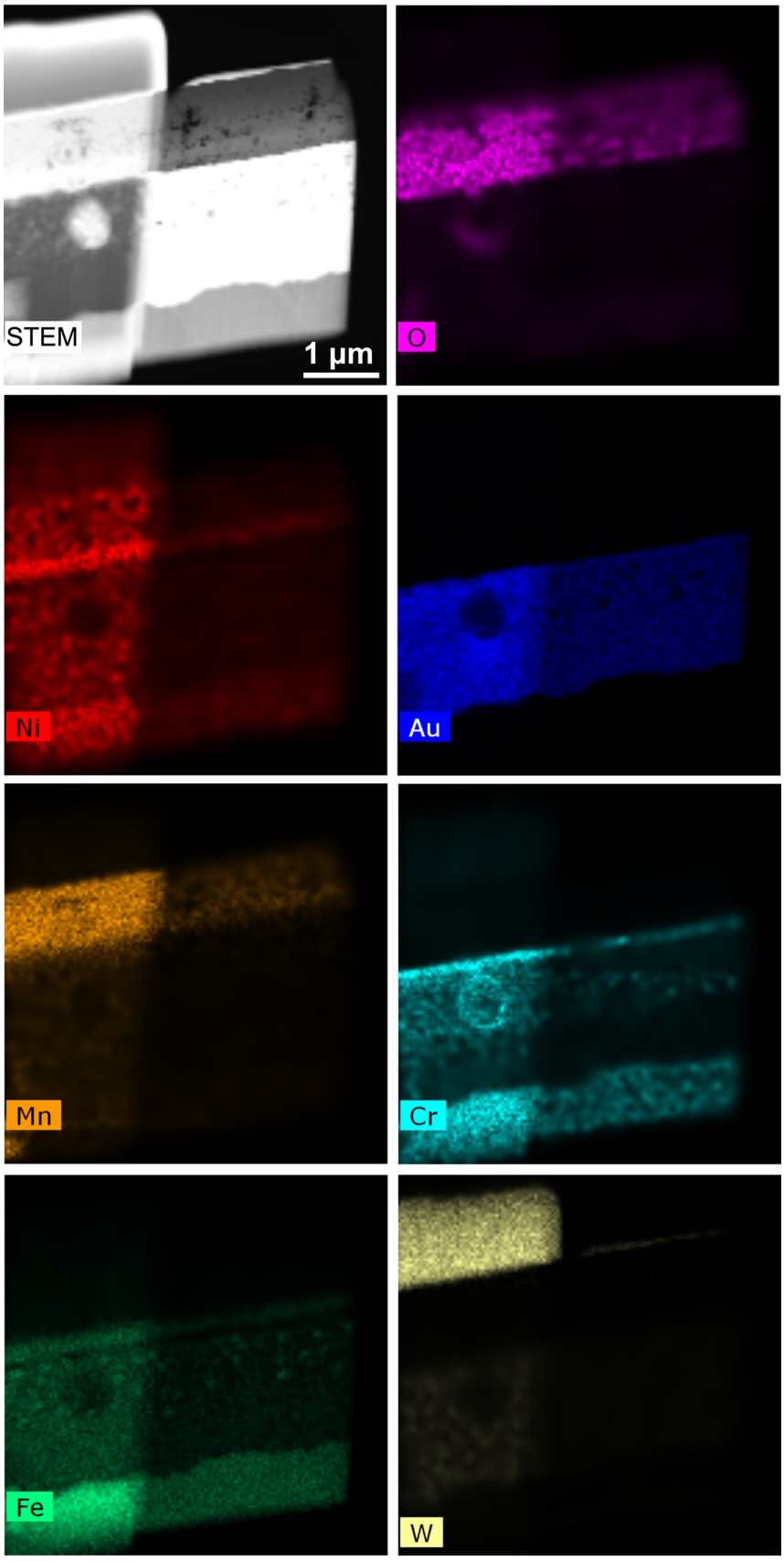

Fig. 11. STEM and STEM/EDX images of LNMO20L lamella.

An equivalent circuit for fitting the impedance data is shown in Fig. 6. Here, R_{EL} represents the electrolyte resistance, while R_{SEI} and the constant-phase element CPE_{SEI} stand for the resistance and the capacitance of the solid electrolyte interphase on the lithium anode. The impedance of the constant-phase element (CPE) is given by $Z_{CPE} = \frac{1}{Q} \cdot (i\omega)^{-n}$ with $n \leq 1$. The capacitance of the constant phase elements was calculated using the Brug [17] formula $C_{CPE} = \left[Q \cdot \left(\frac{1}{R}\right)^{\alpha-1}\right]^{1/\alpha}$. $R_{interlayer}$ and $CPE_{interlayer}$ represent the resistance and the capacitance of interlayer(s) in the LNMO half cell. R_{CT} denotes the charge-transfer resistance in the LNMO half cell, and CPE_{DL} stands for the corresponding double-layer capacitance. Finally, CPE_L represents Li diffusion in LNMO. A typical fit result is shown in Fig. 7.

The resistance of the lithium SEI is in the range of 50 Ωcm^2, and its capacitance is around 2 μFcm^{-2}. When we estimate the thickness of the SEI, d, via the equation $C = \frac{\varepsilon_0 \varepsilon R^A}{d}$ with ε_R = 10-20 (typical range for solid electrolytes), we obtain a value around 6-12 nm. From the resistance value and the estimated thickness value, a specific SEI conductivity of roughly 10^{-9} Scm^{-1} is estimated.

The resistance of the cathodic interlayer(s), $R_{interlayer}$, is about 35 Ωcm^2. This value is consistent with the so-called "solid-liquid interfacial resistance" value in the paper by Mohamedi *et al.* [4] The capacitance of the interlayers is about 0.4 μFcm^{-2}. When we assume again that ε_R = 10-20, we estimate an interlayer thickness of about 30-60 nm and a specific interlayer conductivity of about 10^{-8} Scm^{-1}. The charge transfer resistance R_{CT} is in the range of 50 Ωcm^2 in the voltage range around 4.7 V. The corresponding double layer capacitance is about 30.0 μFcm^{-2}, which is a reasonable value. The charge transfer resistance and the interlayer resistance of LNMO20L are plotted versus cell voltage in Fig. 8. As expected, the interlayer resistance exhibits a weak voltage dependence.

3.4. ToF-SIMS and STEM/EDX Analysis

After finalizing the EIS measurements, the cells were completely discharged, disassembled, and the LNMO films were rinsed with ethanol. Then the films were investigated by means of ToF-SIMS and STEM-EDX.

Representative ToF-SIMS element profiles are shown in Fig. 9. An interlayer on the LNMO surface (SEI layer) could be clearly detected via $H_2P^+$and H_2CO^+ signals originating from the decomposition of PF_6^- anions and of organic carbonates, respectively. The length scale of the H_2P^+ intensity decay is around 50 nm for both LNMO10L and LNMO20L films, which corresponds nicely to the LNMO interlayer thickness estimated from the impedance data. Here, we note that also the results of several other studies point to SEI formation on LNMO particle in composite electrodes [11,12]. The degradation of the electrolyte is initiated by the formation of PF_5 and LiF, when traces of H_2O are present. PF_5 catalyzes the reaction of ethyl carbonate to poly(ethylene oxide) and of dimethylcarbonate to ethane and CO_2. Furthermore, hydrolysis of PF_5 produces HF, which decomposes the entire cathode material, leading to the formation of fluorides and oxyfluorides, like LiF, MnF_2, NiF_2 and PF_3O. The H_2CO^+ signal decay length is below 30 nm. In addition, metal cations, such as nickel and manganese, are detected in this outer part of the layer. This suggests that the outer part consists primarily of organic decomposition products and of dissolved nickel and manganese ions.

At the LNMO/gold interface, an interlayer with a thickness in the range of 250 nm is detected by ToF-SIMS, see Fig. 9. This interlayer consists of different metal oxides, in particular iron oxide, chromium oxide, nickel oxide and lithium oxide. We conclude that this interlayer is caused by the diffusion of iron and chromium from the stainless steel substrate through the Au layer. The thickness of this interlayer is much larger than the estimated thickness of the cathodic interlayer from the EIS measurements. In fact, a semicircle in the Nyquist plot caused by such thick layer is clearly *not* detectable. This provides strong indication that the LNMO/Au interlayer is conductive and does not contribute in a significant fashion to the cell impedance.

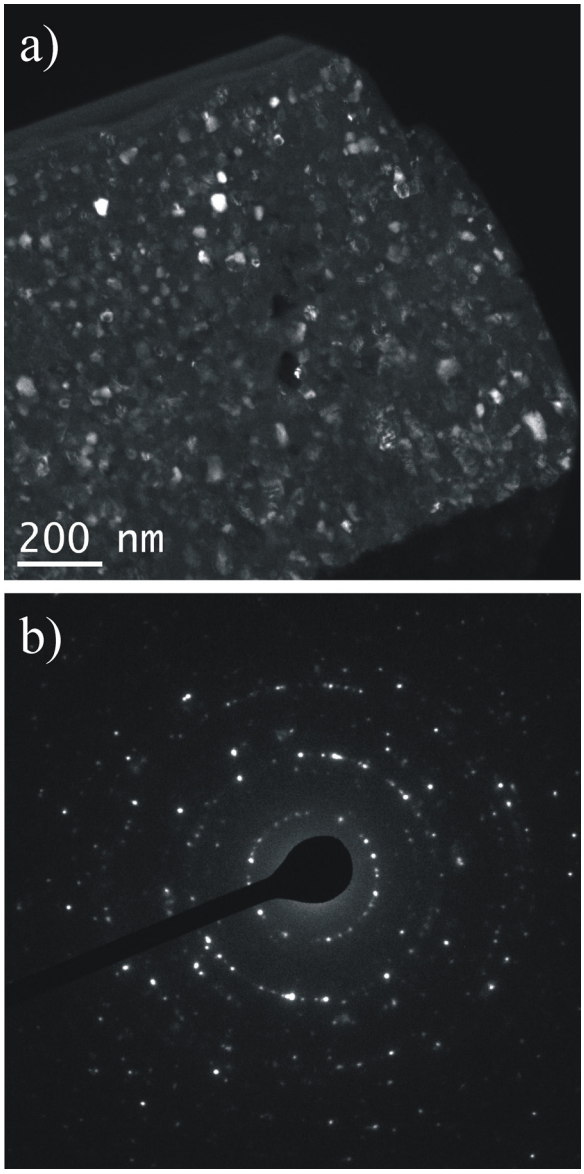

Fig. 12. a) Dark-field TEM micrograph of a LNMO20L lamella showing mainly the LNMO film. b) Selected area electron diffraction (SAED) pattern created with an SAED aperture with a diameter of approximately 150 nm.

Additional information about the LNMO/Au/steel heterostructure was obtained from STEM/EDX studies. To this end, a cross-section TEM lamella was cut out of the LNMO20L sample surfaces using the FIB lift out method. The SEM image of the lamella reveals several interesting features; see Fig. 10. Two different gold layers are clearly distinguishable. The adhesive layer next to the stainless steel substrate is very dense and homogeneous and contains almost no impurities. The second Au layer is more porous and contains iron and chromium impurities, which can be seen in the STEM/EDX data in Fig. 11. The LNMO film itself seems to have some pores or cracks, but its surface is dense. A representative dark-field TEM micrograph of the LNMO film selecting several reflections with the objective aperture and a selected area electron diffraction

pattern are shown in Fig. 12a and b. The dark-field image presents a grainy composition of the LNMO film. Furthermore the diffraction pattern exhibits a polycrystalline structure of the LNMO film. The STEM/EDX pictures shown in Fig. 11 reveal the existence of a very thin chromium oxide layer (< 10 nm) between the mixed oxide interlayer and the gold and confirm the existence of the mixed oxide interlayer (thickness around 250 nm).

4. Conclusions

Thin films of $LiNi_{0.5}Mn_{1.5}O_4$ were prepared via a sol-gel method and were spin-coated onto gold-coated stainless steel substrates. Films with a thickness in the range of 1 μm exhibit a discharge capacity close to the theoretical one.

Electrochemical impedance spectra point to the existence of an interlayer in the cathodic multilayer structure with a thickness in the range of 30-60 nm and with a resistance of about 35 Ωcm^2. ToF-SIMS profiling of the multilayer structure after the EIS measurements shows that an SEI layer with such a thickness is present on the LMNO surface, which was in contact to the LP30 electrolyte. The SEI layer consists of organic decomposition products as well as of different metal fluorides.

In addition, ToF-SIMS and STEM/EDX reveal the existence of a mixed oxide interlayer at the LNMO/Au interface. The formation of this layer is caused by the diffusion of iron and chromium from the stainless steel substrate through the Au layer. The layer is conductive and does not contribute significantly to the cell impedance.

We emphasize that the structural and chemical information from ToF-SIMS and STEM/EDX is essential for understanding the influence of interlayers on the electrochemical performance of thin-film batteries. In particular, interlayers between thin films of active materials and current collectors are often not considered in much detail. In the future, further studies of solid electrolyte interphases and of other interlayers on high-voltage cathode materials should be carried out in order to obtain information about the influence of the inter-layers on the long-term cycling performance of the high-voltage cathode materials.

References

[1] A. Kraytsberg, Y. Ein-Eli, Higher, Stronger, Better . . .A Review of 5 Volt Cathode Materials;1; for Advanced Lithium-Ion Batteries, Advanced Energy Materials 2 (2012) 922.
[2] A. Patil, V. Patil, D.W. Shin, J.-W. Choi, D.-S. Paik, S.-J. Yoon, Issue and challenges facing rechargeable thin film lithium batteries, Materials Research Bulletin 43 (2008) 1913.
[3] K.M. Shaju, P.G. Bruce, Nano-$LiNi_{0.5}Mn_{1.5}O_4$ spinel: a high power electrode for Li-ion batteries, Dalton Trans. 40 (2008) 5471.
[4] Y.K. Yoon, C.W. Park, H.Y. Ahn, D.H. Kim, Y.S. Lee, J. Kim, Synthesis and characterization of spinel type high-power cathode materials Li $M_xMn_{2-x}O_4$ (M = Ni, Co, Cr), Journal of Physics and Chemistry of Solids 68 (2007) 780.
[5] M. Mohamedi, M. Makino, K. Dokko, T. Itoh, I. Uchida, Electrochemical investigation of $LiNi_{0.5}Mn_{1.5}O_4$ thin film intercalation electrodes, Electrochimica Acta 48 (2002) 79.
[6] L. Baggetto, R.R. Unocic, N.J. Dudney, G.M. Veith, Fabrication and characterization of Li-Mn-Ni-O sputtered thin film high voltage cathodes for Li-ion batteries, Journal of Power Sources 211 (2012) 108.
[7] H. Liu, Y.P. Wu, E. Rahm, R. Holze, H.Q. Wu, Cathode materials for lithium ion batteries prepared by sol-gel methods, Journal of Solid State Electrochemistry 8 (2004) 466.
[8] Y.H. Rho, K. Kanamura, M. Fujisaki, J. Hamagami, S. Suda, T. Umegaki, Preparation of $Li_4Ti_5O_{12}$ and $LiCoO_2$ thin film electrodes from precursors obtained by sol–gel method, Solid State Ionics 151 (2002) 151.
[9] K. Hoshina, K. Yoshima, M. Kotobuki, K. Kanamura, Fabrication of $LiNi_{0.5}Mn_{1.5}O_4$ thinfilm cathode by PVP sol–gel process and its application of all-solid-state lithium ion batteries using $Li_{1+x}AlxTi_{2-x}(PO_4)_3$ solid electrolyte, Solid State Ionics 209–210 (2012) 30.
[10] J.C. Arrebola, A. Caballero, L. Hernán, M. Melero, J. Morales, E.R. Castellón, Electrochemical properties of $LiNi_{0.5}Mn_{1.5}O_4$ films prepared by spin-coating deposition, Journal of Power Sources 162 (2006) 606.
[11] J.-H. Kim, N.P.W. Pieczonka, Z. Li, Y. Wua, B.R. Powell, Understanding the capacity fading mechanism in $LiNi_{0.5}Mn_{1.5}O_4$/graphite Li-ion batteries, Electrochimica Acta 90 (2013) 556.
[12] N.P.W. Pieczonka, Z. Liu, P. Lu, K.L. Olson, J. Moote, B.R. Powell, J.-H. Kim, Understanding Transition-Metal Dissolution Behavior in $LiNi_{0.5}Mn_{1.5}O_4$ High-Voltage Spinel for Lithium Ion Batteries, J. Phys. Chem. C 117 (2013) 15947.
[13] N.P.W. Pieczonka, L. Yang, M.P. Balogh, B.R. Powell, K. Chemelewski, A. Manthiram, S.A. Krachkovskiy, G.R. Goward, M. Liu, J.-H. Kim, Impact of Lithium Bis(oxalate)borate Electrolyte Additive on the Performance of High-Voltage Spinel/Graphite Li-Ion Batteries, J. Phys. Chem. C 117 (2013) 22603.
[14] K.J. Carroll, M.-C. Yang, G.M. Veith, N.J. Dudneyc, Y.S. Meng, Intrinsic Surface Stability in $LiMn_{2-x}Ni_xO_{4-(}$ (x = 0.45, 0.5) High Voltage Spinel Materials for Lithium Ion Batteries, Electrochem. Solid-State Lett. 15 (2012) A72.
[15] N.S. Norberg, S.F. Lux, R. Kostecki, Interfacial side-reactions at a $LiNi_{0.5}Mn_{1.5}O_4$ electrode in organic carbonate-based electrolytes, Electrochemistry Communications 34 (2013) 29.
[16] L.H. Chi, N.N. Dinh, S. Brutti, B. Scrosati, Synthesis, characterization and electrochemical properties of 4.8 V $LiNi_{0.5}Mn_{1.5}O_4$ cathode material in lithium-ion batteries, Electrochimica Acta 55 (2010) 5110.
[17] G.J. Brug, A.L.G. Van Den Eeden, M. Sluyters-Rehbach, J.H. Sluyters, The analysis of electrode impedances complicated by the presence of a constant phase element, Journal of Electroanalytical Chemistry 176 (1984) 275.